# Towards Describing Crouzon Syndrome via a Craniofacial Atlas

Hildur Ólafsdóttir[1], Tron Darvann[1,2], Estanislao Oubel[3], Alejandro F. Frangi[3], Nuno V. Hermann[2,4], Bjarne K. Ersbøll[1], and Chad A. Perlyn[5]

[1] Informatics and Mathematical Modelling, Technical University of Denmark, ho@imm.dtu.dk
[2] 3D-Laboratory, School of Dentistry, University of Copenhagen; Copenhagen University Hospital
[3] Computational Imaging Lab, Department of Technology - D.326, Pompeu Fabra University, Barcelona
[4] Department of Pediatric Dentistry and Clinical Genetics, School of Dentistry, Faculty of Health Sciences, University of Copenhagen
[5] Division of Plastic Surgery, Washington University School of Medicine

## 1 Introduction

Crouzon syndrome was first described nearly a century ago when calvarial deformities, facial anomalies, and abnormal protrusion of the eyeball were reported in a mother and her son [1]. Later, the condition was characterized as a constellation of premature fusion of the cranial sutures (craniosynostosis), orbital deformity, maxillary hypoplasia, beaked nose, overcrowding of teeth, and high arched or cleft palate. Identification of heterozygous mutations in the gene encoding *fibroblast growth factor receptor type 2* (FGFR2) have been found responsible for Crouzon syndrome [2]. Recently a mouse model was created to study one of these mutations ($\text{FGFR2}^{\text{Cys342Tyr}}$)[3]. This model allows for detailed examination of the craniofacial growth disturbances. The goal of this study is to automatically assess, visualise and statistically analyse these deviations in a set of adult wild-type (normal) mice and mice with Crouzon syndrome. This paper presents the preliminary steps towards these goals. Firstly, the construction of a nonrigid craniofacial wild-type (WT) mouse atlas. Secondly, the estimation of deformation fields from the atlas to all subjects using nonrigid registration.

The outline of the paper is the following. In the next section, data acquisition and methodology will be discussed. Section 3 presents the experimental results in terms of qualitative and quantitative, landmark-based registration accuracy. Section 4 provides a discussion of the results and conclusions.

## 2 Methods and Materials

### 2.1 Data

Production of the $\text{FGFR2}^{C342Y/+}$ and $\text{FGFR2}^{C342Y/C342Y}$ mutant mouse (Crouzon mouse) has been previously described [3]. All procedures were carried out in

agreement with the United Kingdom Animals (Scientific Procedures) Act, guidelines of the Home Office, and regulations of the University of Oxford. Mutant mice of breeding age were determined by phenotype.

For three-dimensional (3D) CT scanning, 10 WT and 10 $FGFR2^{C342Y/+}$ specimens at six weeks of age (42 days) were sacrificed using Schedule I methods and fixed in 95% ethanol. They were sealed in conical tubes and shipped to the Micro CT imaging facility at the University of Utah. Images of the skull were obtained at approximately $46\mu m \times 46\mu m \times 46\mu m$ resolution using a General Electric Medical Systems EVS-RS9 Micro CT scanner. Figure 1 shows an example of the mice and imaging data appearance.

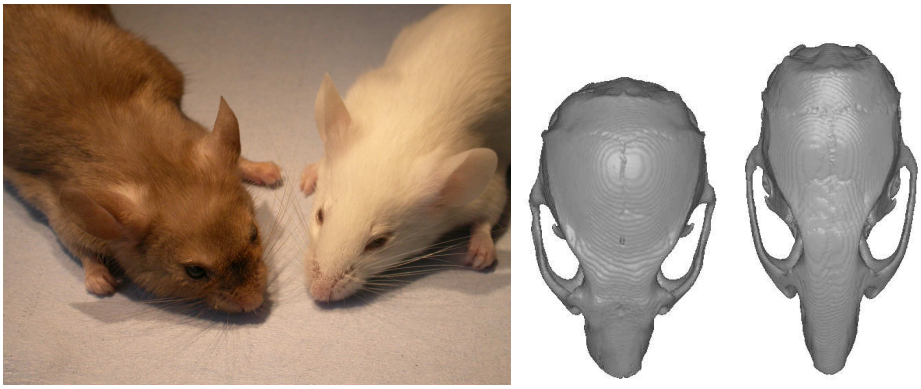

(a) (b) (c)

**Fig. 1.** (a) Photo of a Crouzon mouse (left) and a WT mouse (right). Skull surfaces extracted from CT images of (b) a Crouzon mouse, (c) WT mouse.

### 2.2 Nonrigid registration

The goal of image registration is to warp one image into the coordinate system of another using an optimal transformation $\mathbf{T}(x, y, z) \mapsto (x', y', z')$. A basic image registration algorithm requires the following:

- A transformation type.
- A measure of image similarity.
- An optimisation method to optimise the transformation parameters with respect to the similarity measure.

In this study the FFD-based nonrigid registration algorithm presented in [4] was adopted. In this approach, the transformation consists of both a global and a local model, i.e.

$$\mathbf{T}(x, y, z) = \mathbf{T}_{global}(x, y, z) + \mathbf{T}_{local}(x, y, z). \quad (1)$$

The global transformation model describes the overall difference between the two images. This is achieved by an affine transformation. In this study, the affine transformation was defined by rotation and translation in addition to anisotropic scaling since the largest changes between the two groups stem from the differences in aspect ratio. This gives an affine transformation with 9 degrees of freedom. In this way, the largest part of the differences between the two groups of mice is covered by the affine registration.

However, local differences between the groups still remain. This calls for a nonrigid (and nonaffine), local transformation model. The FFD model based on B-splines has proven to be a powerful tool when modelling such deformations. In 3D, the FFD is defined by an $n_x \times n_y \times n_z$ mesh of control points $\mathbf{\Phi}$ with spacing $(\delta_x, \delta_y, \delta_z)$. The underlying image is then deformed by manipulating the mesh of control points. The FFD model can be written as the tensor product of the one-dimensional (1D) cubic B-splines

$$\mathbf{T}_{local}(x,y,z) = \sum_{l=0}^{3}\sum_{m=0}^{3}\sum_{n=0}^{3} B_l(u)B_m(v)B_n(w)\phi_{i+l,j+m,k+n} \tag{2}$$

where $i = \lfloor x/n_x \rfloor - 1, j = \lfloor y/n_y \rfloor - 1, k = \lfloor z/n_z \rfloor - 1, u = x/n_x - \lfloor x/n_x \rfloor, v = y/n_y - \lfloor y/n_y \rfloor$ and $w = z/n_z - \lfloor z/n_z \rfloor$

$B_r$ represents the $r$th basis function of the B-spline

$$\begin{aligned} B_0(u) &= (1-u)^3/6 \\ B_1(u) &= (3u^3 - 6u^2 + 4)/6 \\ B_2(u) &= (-3u^3 + 3u^3 + 3u + 1)/6 \\ B_3(u) &= u^3/6. \end{aligned}$$

The similarity metrics tested in this study were Sum of Squared Differences (SSD), Cross Correlation (CC) and Normalised Mutual Information (NMI). In short, NMI outperformed the other two and was therefore used in the remaining experiments. A gradient descent approach was used to optimise the similarity measure. An implementation of the algorithm by Rueckert[6] [4] was applied.

### 2.3 Atlas construction

An anatomical atlas was constructed from the set of WT mice in an iterative manner using nonrigid registration. The procedure is listed in Table 1.

Lines 6 and 7 from table 1 are intended to reduce the bias towards the choice of reference subject as done with good results in [5]. Figure 2 shows the resulting atlas in three different views and as a surface extracted from the volume.

[6] http://www.doc.ic.ac.uk/∼dr/software/

**Table 1.** Atlas construction

| |
|---|
| 1 atlas ← a selected reference subject from the set of WT mice |
| 2 **do** |
| 3 Nonrigidly register all WT mice to atlas |
| 4 atlas ← Average of all registered mice |
| 5 **until** atlas stops changing |
| 6 Nonrigidly register atlas to all WT mice |
| 7 Deform atlas by $\bar{\mathbf{d}}$ = the average deformation obtained in step 6 |

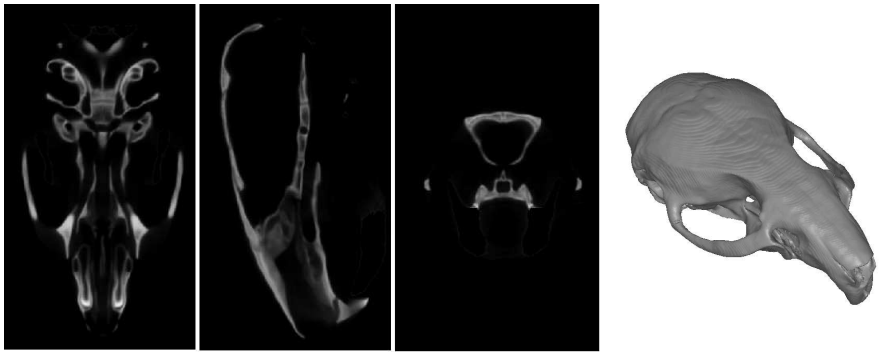

(a) (b) (c) (d)

**Fig. 2.** The craniofacial, nonrigid mouse atlas in (a) axial, (b) sagittal and (c) coronal view. (d): 3D surface view of the atlas.

## 3 Results

### 3.1 Registration accuracy

To assess the craniofacial deviations caused by the Crouzon syndrome, the atlas in Figure 2 was registered to all subjects (WT and Crouzon cases). The registration accuracy was examined both qualitatively and quantitatively. Figure 3 shows difference images between one of the Crouzon cases and the atlas before and after registration. Figure 4 shows the closest point difference between the atlas and one of the Crouzon cases before and after registration, as a color overlay on the two surfaces. To provide a quantitative analysis of the registration accuracy, surfaces were extracted from the images and two independent observers put 26 anatomical landmark on all the cases. Using the optimal deformations, the landmarks were also obtained automatically by propagating the atlas landmarks to each of the remaining subjects. Figure 5 shows the landmark errors, i.e. point to point distances between the two observers and between the automatically generated landmarks and each of the observers.

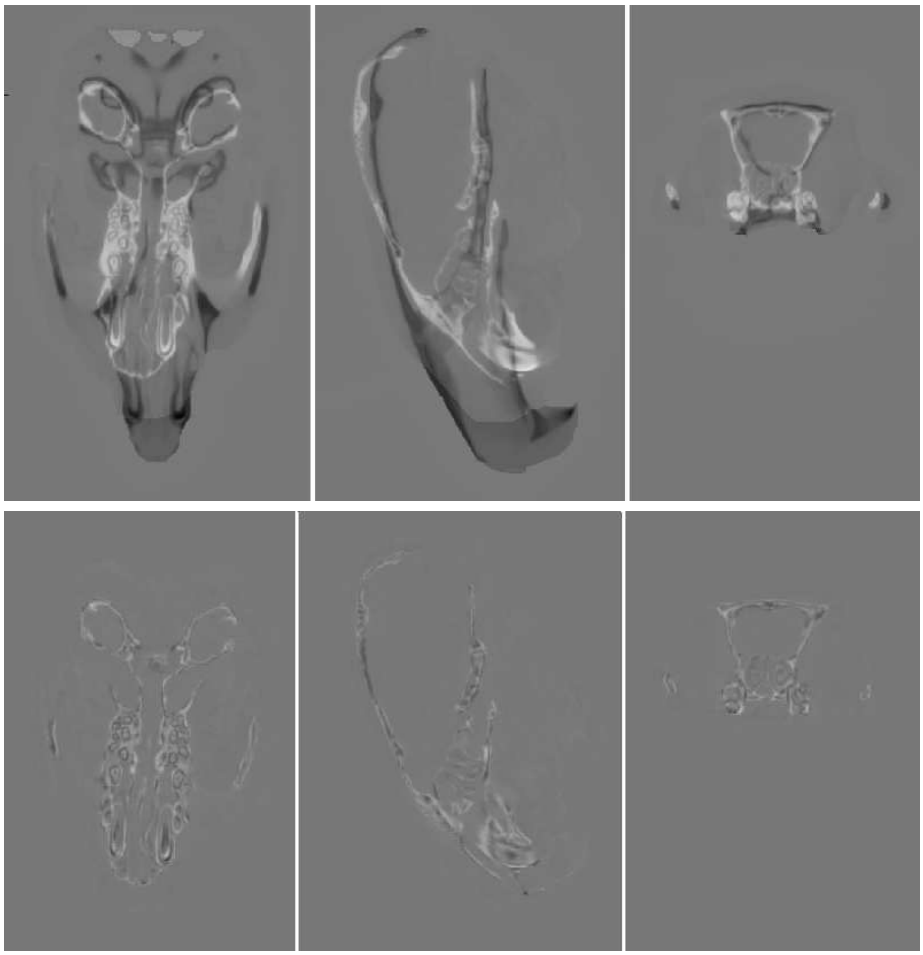

(a) (b) (c)

**Fig. 3.** Difference images before (top row) and after (bottom row) registration of the atlas to a Crouzon mouse in (a) axial, (b) sagittal and (c) coronal view.

## 4 Discussion

Figure 3 indicates that the differences between the atlas and the Crouzon case have been compensated for during the registration. In the top row, one can observe large global differences especially in the length and width of the skull. Locally, the shape of the nose and the upper jaw is very different. All these differences and many more, not seen in this figure have been compensated for by the registration (both the global and the local one). Figure 4 gives a semi-quantitative impression of the registration accuracy. Before registration, the distance between the surfaces of the atlas and the Crouzon case reach over 0.75

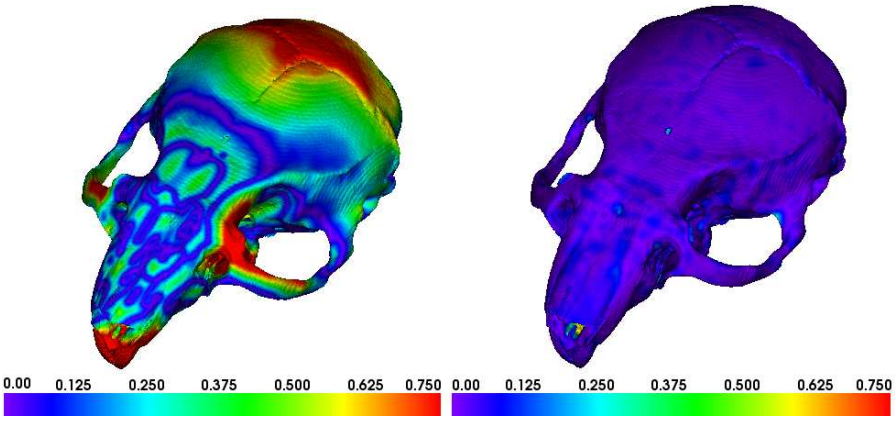


(a) (b)

**Fig. 4.** Surface views with color coding denoting closest point difference (in mm) between the surface of the atlas and the Crouzon mouse (a) before and (b) after registration.

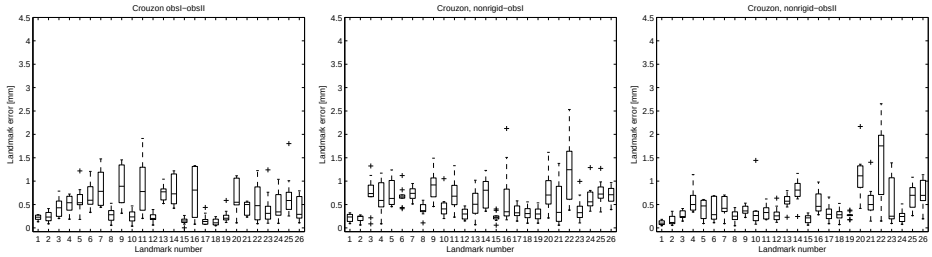


(a) (b) (c)

**Fig. 5.** Landmark errors for Crouzon cases. (a) Interobserver errors, (b)Automatic to observer I, (c) Automatic to observer II.

mm. After affine and nonrigid registration, these differences have been reduced to around 0.1-0.2 mm. A further inspection of the accuracy is given in Figure 5. The landmark errors indicate that the automatic approach is just as good as the manual annotations and even more consistent. However, one landmark (number 22) seems to give problems. This landmark is placed where the frontal nasal suture and sagittal suture meet. The explanation might be that image information is not sufficient for these sutures to match accurately. It was also noted that in some of the Crouzon cases they are hardly visible. Overall, the accuracy is considered to be good. This allows for automatic assessment of the deviations in Crouzon subjects in terms of morphological measuremnts on the skull. Further, the nonrigid registration parameters serve as a good basis for statistical analysis of the deformations between and within the two groups.

## 5 Conclusion

In summary, this paper has presented the construction of a nonrigid craniofacial wild-type mouse atlas. Furthermore, the atlas has successfully been registered to wild-type mice as well as Crouzon mice. Provided the accurate registrations, it is now possible to automatically assess the growth deviations in Crouzon subjects and carry out statistical analyses of the nonrigid deformations.

## References


1. Crouzon, O.: Dysostose craniofaciale héréditère. Bull Mem Sòc Méd Hôp Paris **33** (1915) 545–55
2. Reardon, W., Winter, R.M., Rutland, P., Pulleyn, L.J., Jones, B.M., Malcolm, S.: Mutations in the fibroblast growth factor receptor 2 gene cause Crouzon syndrome. Nat Genet **8** (1994) 98–103
3. Eswarakumar, V.P., Horowitz, M.C., Locklin, R., Morriss-Kay, G.M., Lonai, P.: A gain-of-function mutation of fgfr2c demonstrates the roles of this receptor variant in osteogenesis. Proc Natl Acad Sci, U.S.A. **101** (2004) 12555–60
4. Rueckert, D., Sonoda, L.I., Hayes, C., Hill, D.L.G., Leach, M.O., Hawkes, D.J.: Nonrigid registration using free-form deformations: application to breast MR images. Medical Imaging, IEEE Trans. on **18**(8) (1999) 712–721
5. Rueckert, D., Frangi, A.F., Schnabel, J.A.: Automatic construction of 3D statistical deformation models of the brain using nonrigid registration. IEEE Transactions on Medical Imaging **22**(8) (2003) 1014–1025